Supporting Information

Keegan et al. 10.1073/pnas.1405397111

SI Materials and Methods

Firn Core Analysis. We examined the stratigraphy of six firn cores, identified as Summit-2007, Summit-2010, D4, ACT 3, NEEM 2008 S1, and NEEM 2009 S2 in this paper, which cover a broad spatial extent over the Greenland Ice Sheet (GIS) (Fig. S1). A distinct refrozen melt layer was visible in each core, denoting a melt event in each core. Using depth–age scales for each site, we identified the ages of the melt layers (Table S1). The melt layer in both NEEM firn cores date to mid-1888, which seems reasonable, because the melt water would need to percolate to a firn layer cold enough to allow refreezing. Since the NEEM site is lower in elevation and warmer than Summit, it is reasonable to expect the melt water to percolate into the 1888 firn layers before refreezing. Annual snow accumulation rates at D4 (413 kg m^{-2} y^{-1}) and ACT 3 (662 kg m^{-2} y^{-1}) are much higher than the modern rates at Summit (223 kg m^{-2} y^{-1}) and NEEM (207 kg m^{-2} y^{-1}), so melt penetration at these sites is limited to a few months of record at most. Lastly, a vertical profile sample of the near-surface snow from Summit Greenland, which incorporated the 2012 melt layer, also was analyzed.

In this paper, we focus on the chemical and elemental analysis of the Summit-2010 firn core and Summit-2012 near-surface sample, because Summit is the least likely site to experience melt during a widespread melt event due to its position at the summit of the GIS. We measured black carbon (BC), ammonium ion as a proxy of forest fires (1), and $\delta^{18}O$ as a proxy for temperature (2) (Fig. S2). We use an SP2 intercavity laser-based instrument for measuring BC with a detection limit of ∼0.02 ng g^{-1} (3), a Picarro L2130-i cavity-ring-down-based laser instrument to measure the stable water isotopes ($\delta^{18}O$) (4), and fluorimetry to measure the ammonium concentrations (5). In Fig. S2, we confirm that the temperature and $\delta^{18}O$ trends are related at Summit for the recent past.

To clearly demonstrate the effect of high concentrations of BC and ammonium, as well as the ratio of $\delta^{18}O$ on the same scale, we plotted the three variables together on a normalized scale. The records were normalized by the minimum and maximum values of the full record (1750–2010, 2012 A.D.) for each variable (Fig. S3), which were 0.023 ng g^{-1} and 14.4 ng g^{-1} of BC, 0.003 μM and 8.86 μM of ammonium, and −37.6‰ and −30.6‰ $\delta^{18}O$, respectively. These normalized values were then plotted on a scale of 0–1 for each time series shown in Fig. 2 *A*–*D*. The average concentrations of BC and ammonium from the 2012 surface sample were also normalized with the maximum and minimum values from their respective full records (1750–2010, 2012 A.D.), and plotted in the bar graph in Fig. 2*E*. Stable water isotopes were not measured on the 2012 surface sample, so the average temperature measured at Summit from June–August of 2012 (−12.4 °C) was compared with average summer temperatures in the recent history and found to be similar to that of 2010 (−12.2 °C) (6). Therefore, we assigned the 2012 surface sample a normalized $\delta^{18}O$ value equivalent to that of 2010 (0.86).

To investigate the source of the BC found at Summit, we found data showing large-scale forest fires burning in North America (7, 8) and Siberia (9) in late June and early July of 2012, respectively. We identified potential source regions of BC using a HYSPLIT 5-d back-trajectory model of particles arriving at Summit during the time period of June 28 through July 12, 2012 (Fig. S4). In Fig. S4, the blue dots indicate the origin of particles arriving at Summit June 28 through July 3 and red dots indicate the origin of those arriving July 7–12. Therefore, Fig. S4 demonstrates that air masses from both North America and Siberia reached Summit during this time, which could have carried BC particles.

Melt Calculations. The amount of energy needed to generate surface melt and percolation was calculated from Dingman's equations (10) for the warming phase (Q_{cc}), ripening phase (Q_{m2}), and output phase (Q_{m3})

$$Q_{cc} = -c_i \rho_w h_m (T_s - T_m) \quad \textbf{[S1]}$$

$$Q_{m2} = \theta_{ret} h_s \rho_w \lambda_f \quad \textbf{[S2]}$$

$$Q_{m3} = (h_m - h_{wret}) \rho_w \lambda_f, \quad \textbf{[S3]}$$

where c_i is the specific heat capacity of ice (2.102 kJ kg^{-1} K^{-1}), ρ_w is the density of water (1000 kg m^{-3}), h_m is the snowpack water equivalent (meters), T_S is the average temperature of the snow, T_m is the melting temperature (273 K), θ_{ret} is the maximum volumetric water content, h_s is the snow depth (meters), λ_f is the latent heat of fusion (334 kJ kg^{-1}), and h_{wret} is the liquid water retaining capacity of the snowpack (meters). The θ_{ret} can be calculated from the empirical relationship

$$\theta_{ret} = -0.0745\left(\frac{\rho_s}{\rho_w}\right) + 0.000267\left(\frac{\rho_s}{\rho_w}\right)^2, \quad \textbf{[S4]}$$

where ρ_S is the snowpack density. The h_{wret} can be calculated from the relationship

$$h_{wret} = \theta_{ret} h_S. \quad \textbf{[S5]}$$

The snowpack water equivalent depth, h_m, can be determined from

$$h_w = \frac{\rho_S h_S}{\rho_w}. \quad \textbf{[S6]}$$

Substituting Equations **S4**–**S6** into Equations **S1**–**S3**, allows us to solve Equations **S1**–**S3** for the energy required. The summation of Q_{cc}, Q_{m2}, and Q_{m3} gives the theoretical amount of energy required for surface melt and percolation (10).

To determine the amount of energy available at the surface, we calculated the surface energy balance from

$$S = (1 - \alpha) K_{in} + L_{in} - L_{out} + H + LE, \quad \textbf{[S7]}$$

where S is the energy flux at the snow surface (W m^{-2}), α is the albedo, K_{in} is the incoming shortwave radiation, L_{in} is the incoming longwave radiation, L_{out} is the outgoing longwave radiation, H is the turbulent sensible heat flux, and LE is the turbulent latent heat flux (11).

Given an average T_S of −15 °C, h_S of 1 cm, and ρ_S of 300 kg m^{-3}, it requires 1.1 MJ m^{-2} of energy to cause surface melt and percolation. Since the melt layers are ∼1–2 cm thick, it is reasonable to expect surface snow on the order of 1 cm to melt (h_S).

The amount of energy available at the surface for melting in July 2012 was calculated using the average daily incoming radiation, 409 W m^{-2}, an albedo that includes an average amount of coarsening, 0.77, longwave radiation of 205 W m^{-2}, outgoing radiation of 317 W m^{-2}, sensible heat flux of 4 W m^{-2}, and latent heat flux of 3 W m^{-2} (11), and, over 7 h, gives 0.94 MJ m^{-2} of

energy. The concentration of BC at the surface in 2012 provided at least 1% reduction in albedo (12), and surface snow metamorphism due to warmer temperatures provided ~5% reduction in albedo (13). These two effects combined (~6% reduction in albedo) provided at least 0.3 MJ m^{-2} of energy, tipping the surface energy available over the 1.1 MJ m^{-2} threshold to 1.24 MJ m^{-2} and thus allowing melting to occur.

Modeling Future Widespread Melt. To model how the probability of widespread melt events will change in the future due to climate change, the forecasted rise in temperature (14) and increase in forest fire frequency (15) were used. To incorporate a warming average summer temperature in the Arctic, the average energy required to cause melt and percolation was calculated with the Intergovernmental Panel on Climate Change AR5 scenarios predicting Arctic summer temperature increases of 2 °C and 9 °C by 2100 (14).

The projected energy available at the surface was calculated for four scenarios: 2 °C end-of-century temperature rise, 2 °C rise with increasing forest fire frequency, 9 °C end-of-century temperature rise, and 9 °C rise with increasing forest fire frequency. We calculated the temperature effect on the incoming and outgoing longwave radiation, as well as on the albedo for 5-y time steps in each of the four scenarios. The albedo will decrease by ~3% per °C rise in average temperature due to snow metamorphism at the surface, and will reach a maximum of ~7.5% reduction (13). The increase in available energy was applied to a 10-y dataset of daily summer (June 1 through Aug. 31) net radiation, and the annual average was generated from bootstrapping 1,000 random samples from the dataset with replacement.

BC present at the surface of the ice sheet increases the amount of energy available at the surface by decreasing the albedo by ~1% when present (12, 16). With climate change, it is projected that forest fires frequency will increase twofold to fourfold per °C in warming. We generated a dataset for the effect of BC on the surface energy available by taking the 262-y BC record at Summit and giving a reduction of albedo by 1% to large BC spikes (> 9 ng g^{-1}). Using a doubling in frequency of forest fire BC reaching the GIS per 1 °C, we randomly added large BC events based on the warming to the dataset. For each time step, the datasets were also sampled at random 1,000 times with replacement using the bootstrapping method.

To calculate the probability of widespread melt events occurring through 2100, we combined the 1,000 energy values due to warming with those due to BC and generated a probability that the energy available was greater than the 1.1MJ m^{-2} needed to cause widespread melting events. We performed these calculations for each time step and plotted the probabilities in Fig. 3.

1. Legrand M, De Angelis M, Staffelbach T, Neftel A, Stauffer B (1992) Large perturbations of ammonium and organic acids content in the Summit-Greenland ice core. Fingerprint from forest fires? *Geophys Res Lett* 19(5):473–475.
2. Siegenthaler U, Oeschger H (1980) Correlation of ^{18}O in precipitation with temperature and altitude. *Nature* 285(5763):314–317.
3. McConnell JR, et al. (2007) 20th-century industrial black carbon emissions altered Arctic climate forcing. *Science* 317(5843):1381–1384.
4. Maselli OJ, Fritzsche D, Layman L, McConnell JR, Meyer H (2013) Comparison of water isotope-ratio determinations using two cavity ring-down instruments and classical mass spectrometry in continuous ice-core analysis. *Isotopes Environ Health Stud* 49(3): 387–398.
5. McConnell JR, Lamorey GW, Lambert SW, Taylor KC (2002) Continuous ice-core chemical analyses using inductively coupled plasma mass spectrometry. *Environ Sci Technol* 36(1):7–11.
6. Steffen K, Box J, Abdalati W (1996) Greenland Climate Network: GC-Net (US Army Cold Reg Res Lab, Hanover, NH) CRREL Spec Rep 96-27.
7. NOAA National Climatic Data Center (2012) State of the Climate: Wildfires for June 2012. Available at www.ncdc.noaa.gov/sotc/fire/2012/6. Accessed December 1, 2013.
8. NOAA National Climatic Data Center (2012) State of the Climate: Wildfires for July 2012. Available at www.ncdc.noaa.gov/sotc/fire/2012/7. Accessed December 1, 2013.
9. Earth Observatory NASA (2012) Smoke and fires in Siberia: Natural hazards. Available at http://earthobservatory.nasa.gov/NaturalHazards/view.php?id=78406&eocn=image&eoci=related_image. Accessed March 13, 2014.
10. Dingman L (1994) *Physical Hydrology* (Prentice Hall, Englewood Cliffs, NJ).
11. Cullen N, Steffen K (2001) Unstable near-surface boundary conditions in summer on top of the Greenland ice sheet. *Geophys Res Lett* 28(23):4491–4493.
12. Warren S, Wiscombe W (1980) A model for the spectral albedo of snow. II: Snow containing atmospheric aerosols. *J Atmos Sci* 37(12):2734–2745.
13. Flanner M, Zender C (2006) Linking snowpack microphysics and albedo evolution. *J Geophys Res* 111(D12):D12208.
14. Intergovernmental Panel on Climate Change (2013) *IPCC Fifth Assessment Report, Climate Change 2013: The Physical Science Basis* (Cambridge Univ. Press, Cambridge).
15. Westerling AL, Hidalgo HG, Cayan DR, Swetnam TW (2006) Warming and earlier spring increase western U.S. forest wildfire activity. *Science* 313(5789):940–943.
16. Flanner M, Zender C, Randerson J, Rasch P (2007) Present-day climate forcing and response from black carbon in snow. *J Geophys Res* 112(D11):D11202.

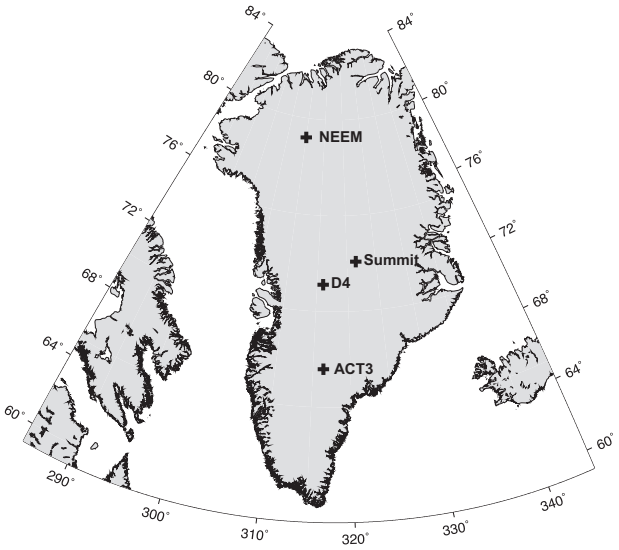

Fig. S1. A map of the four Greenland firn core site locations, which are denoted by black crosses. ACT3 is located at (67.0°N, 43.6°W), D4 is located at (71.4°N, 44.0°W), Summit is located at (72.6°N, 38.5°W), and NEEM is located at (79.0°N, 50.0°W).

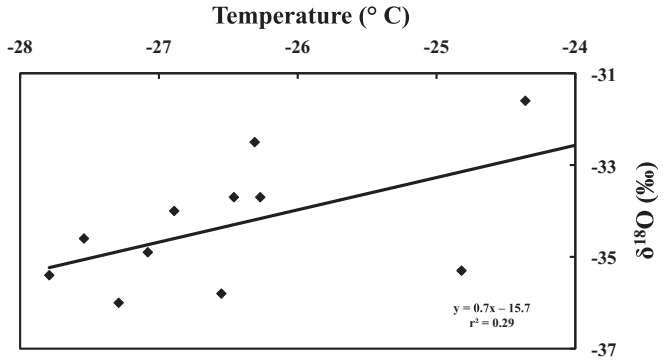

Fig. S2. Annual average temperature vs. annual average $\delta^{18}O$ at Summit, Greenland, from 2000 to 2010. The linear regression line shows a moderate correlation between temperature and $\delta^{18}O$ ($r^2 = 0.29$).

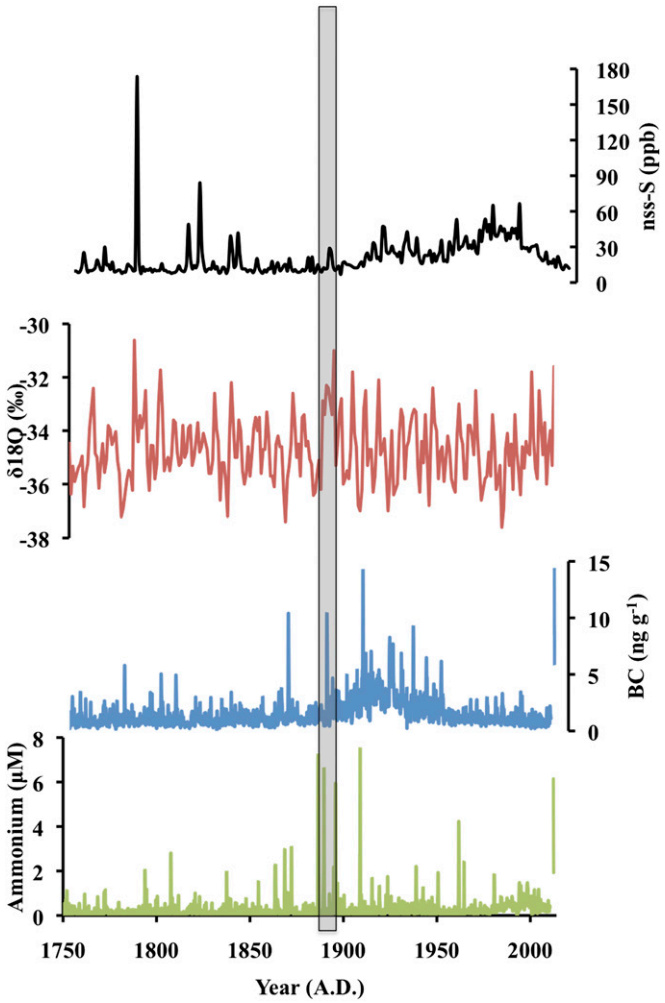

Fig. S3. The non-sea-salt sulfur (nss-S), stable water isotopes ($\delta^{18}O$), BC, and ammonium records from the summit-2010 firn core, as well as BC and ammonium concentrations from the 2012 Summit near-surface sample.

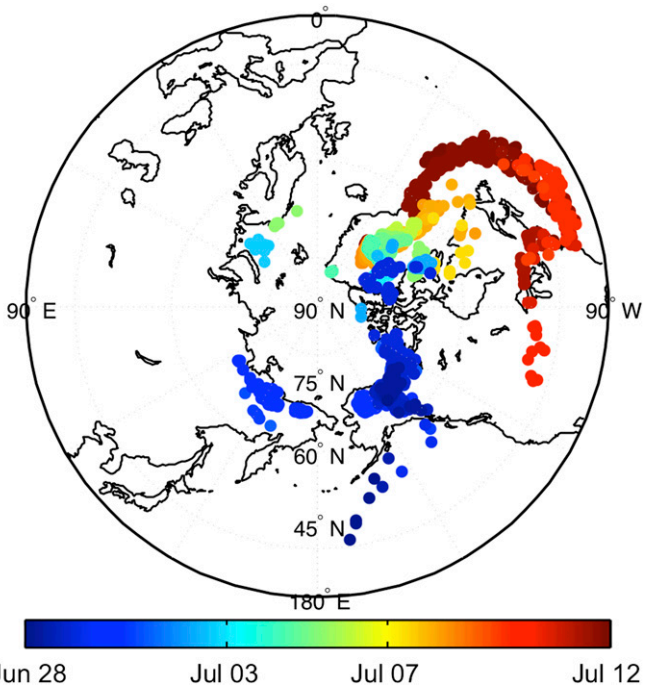

Fig. S4. A plot of particle origin to Summit, Greenland, from June 28 through July 12, 2012, as calculated by HYSPLIT with a 5-d back-trajectory. The shade of the dots indicate the date of landing at Summit, with blue shades showing the origin of particles landing on June 28 through July 3 and red shades on July 7–12.

Table S1. Site, depth, and age of the Greenland 1889 melt layer

Core	Melt depth, meters	Age, A.D.
Summit-2007	47.1	1889.2
Summit-2010	47.0	1889.1
NEEM 2009 S2	43.1	1888.5
NEEM 2008 S1	42.6	1888.5
ACT 3	108.7	1889.3
D4	72.4	1889.4